14th Australasian Fluid Mechanics Conference
Adelaide University, Adelaide, Australia
10-14 December 2001

Numerical Simulation of Membrane Forcing Effects On Synthetic Jet Actuator Flows

S.G. Mallinson⊗ and J.A. Reizes

Faculty of Engineering, University of Technology, Sydney

Broadway NSW 2007 AUSTRALIA

Abstract

Incompressible laminar Navier-Stokes computations of synthetic jet actuator flows have been performed, employing realistic orifice and cavity geometry and membrane forcing characteristics. The external flow-field exhibits periodic vortex shedding from the lip of the orifice exit. A vortex is shed into the cavity from the orifice inlet on the downstroke of the membrane. On the upstroke, this vortex dissipates and there is very little motion near the perimeter of the cavity. The results of a series of simulations suggest a linear relationship between average velocity at the orifice exit and the product of membrane forcing frequency and maximum deflection.

Introduction

Effective implementation of active flow control (AFC) systems requires a clear understanding of the control actuator physics. This study examines the flow produced by a compact, low-power AFC device, the synthetic jet actuator (Fig. 1). For the external flow, it has been found [2,7,9,10,13,14] that: a number of different flow patterns can arise, including periodic vortex shedding (Fig. 1) and a steady turbulent jet (in the far-field); flow reversal occurs only close to the orifice; the pulsations cause rapid entrainment of momentum; the near-field behaviour scales with averaged outflow velocity and forcing frequency; the jets lose their coherency in the far-field; and, it is possible to ignore the cavity in the computations and still achieve reasonable agreement in the far-field. It can be argued that poor agreement in the near-field may be due to ignoring the orifice and cavity regions, which will ultimately determine the outflow properties. There have been several numerical studies of synthetic jets which include these regions. Rizzetta et al [12] and Lee and Goldstein [8] considered 2-D / planar actuator flows and assumed a piston-type boundary condition for membrane motion. Mittal et al [11] used a more realistic membrane motion in a 2-D simulation. Guo and Kral [5] applied a pressure boundary condition upstream of the orifice, which ignores the containment effect provided by the membrane. In all of these studies, the dimensions for the orifice and cavity did not match any experimental configuration.

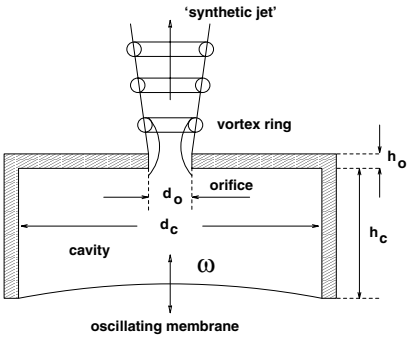

Figure 1: Schematic of idealized operation of a synthetic jet actuator. d_o = orifice diameter, d_c = cavity diameter, h_o = orifice height, h_c = cavity height, Δ_{max} = maximum membrane deflection, $\omega = 2\pi f$, f = forcing frequency.

Here, we employ a computational fluid dynamics code, CFX4.3, to simulate laminar, incompressible synthetic jet actuator flows, including cavity, orifice and external regions. This code has been employed previously to model pulsatile flows and found to compare well with experimental data [6]. The equations are solved using the full Stone method for velocity and the pre-conditioned conjugate gradient method for pressure. Hybrid differencing is used and the pressure correction is performed with the SIMPLEC method. Only circular geometries are considered, which allows us to employ the simplifying assumption of axial symmetry. The dimensions of the actuator are the same as those from our earlier study [9], namely d_o = 0.75 mm, h_o = 1.65 mm, d_c = 36.8 mm and h_c = 1.35 mm.

Numerical Method

The membrane motion is prescribed as a sinusoidal oscillation of the fundamental mode of a membrane clamped firmly around its perimeter [1], and is specified completely by a maximum deflection, Δ_{max}, and a forcing frequency, f. The local deflection, $\Delta(r, t)$, is given by:

$$\frac{\Delta(r,t)}{\Delta_{\max}} = \left[J_0\left(\frac{\lambda r}{a}\right) - \frac{J_0(\lambda)}{I_0(\lambda)} I_0\left(\frac{\lambda r}{a}\right) \right] \sin(\omega t) \qquad (3)$$

where r is the radial distance from the membrane centre, t is time, J_0 is the modified Bessel function of the first kind, I_0 is the Bessel function of the first kind, a is the membrane radius and λ is a dimensionless parameter which depends on the mode. In this case, $\lambda = 10.22^{1/2}$.

A moving mesh boundary condition was implemented, with the location of the mesh points inside the cavity being redistributed using a linear function. The orifice exit plane was set at y = 0. The external field extended to $y / d_o = 45$ and $r / r_o = 50$. The mesh dimensions, N_x and N_y, were 181 x 151 (external), 20 x 25 (orifice) and 110 x 25 (cavity). Power-law stretching was applied near the orifice lip and all other surfaces, with less than five percent change in mesh size between adjacent cells.

Table 1 presents the conditions for the test cases we have considered in this study. All cases assumed laminar flow, which may not necessarily represent the real flows, but will allow us to examine the role of pulsations in the absence of turbulence. The test medium is air, with $\rho = 1.223$ kg m^{-3} and $\mu = 1.7 \times 10^{-5}$ Pa s. The approximate range of Reynolds and Strouhal numbers for this study, based on the average velocity at the centre of the orifice outlet, were 150-900 and 0.03 – 0.3, respectively.

Results and Discussion

Figure 2 presents a time sequence of instantaneous vorticity contour plots of the external, orifice and cavity flow-fields for a single cycle of the membrane. The flow becomes cyclic after the second forcing period, and the instants shown are during the fifth cycle. The results are for case 6, although the other cases exhibit

⊗ present address: Silverbrook Research, Balmain NSW 2041

Case	Δ_{max} (μm)	f (kHz)
1	0.2	0.725
2	0.5	0.725
3	1.0	0.725
4	0.2	1.45
5	0.5	1.45
6	1.0	1.45

Table 1. Membrane forcing parameters for present study.

very similar flow features. Most of the flow in the cavity is concentrated along the centre-line, as found by Mittal et al [11] for 2-D flow, and so we have focused on the region $|r| < 10$ mm.

In the external flow, a vortex pair forms at the start of the cycle and moves away from the orifice under its own momentum. A "satellite" vortex ring breaks away from the main vortex in the latter stages of the cycle (Fig. 2(d)). The breakaway location moves away from the orifice as Δ_{max} and f increase. The flow-field bears a strong resemblance to the idealized flow (Fig. 1) and also to laminar simulations that did not consider the cavity [7,9].

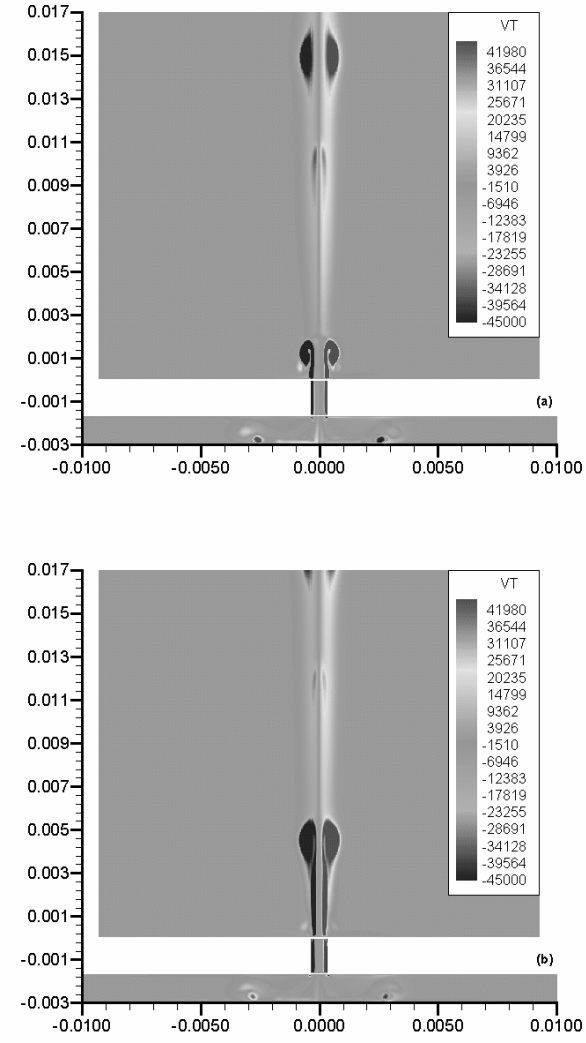

Figure 2. Time-sequence of instantaneous vorticity contours for case 6. (a) $t^* = 5.05$; (b) $t^* = 5.28$. $t^* = t / \tau$, where $\tau = 1 / f$.

Vortex rings form near the bottom and top of the orifice during the exhaust and refill parts of the cycle, respectively, passing

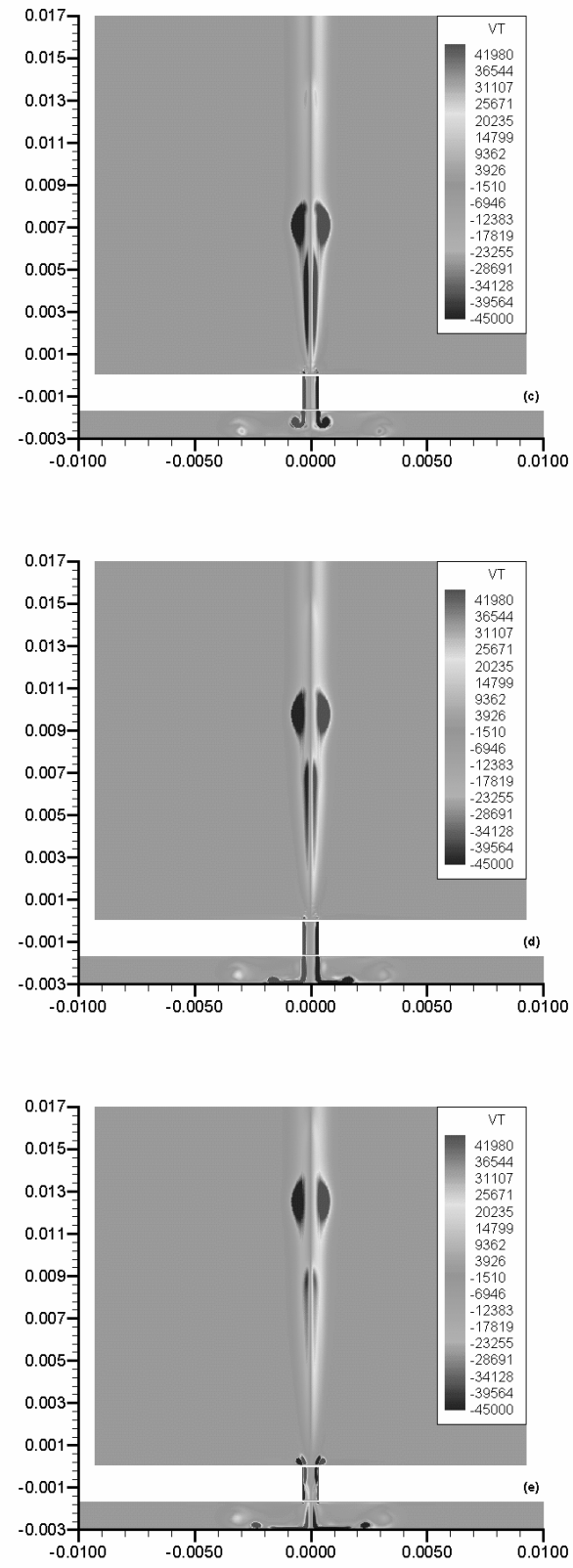

Figure 2. (continued). (c) $t^* = 5.46$; (d) $t^* = 5.66$; (e) $t^* = 5.86$.

along the orifice walls during the cycle. The vortex that forms on the downstroke passes into the cavity and appears to dissipate on the next upstroke. This may be due to the counter-rotating vorticity that is generated by the upstroke of the membrane. The centre-line distributions of stream-wise velocity and pressure are presented in Fig. 3 at the same instants as in Fig. 2. These show a

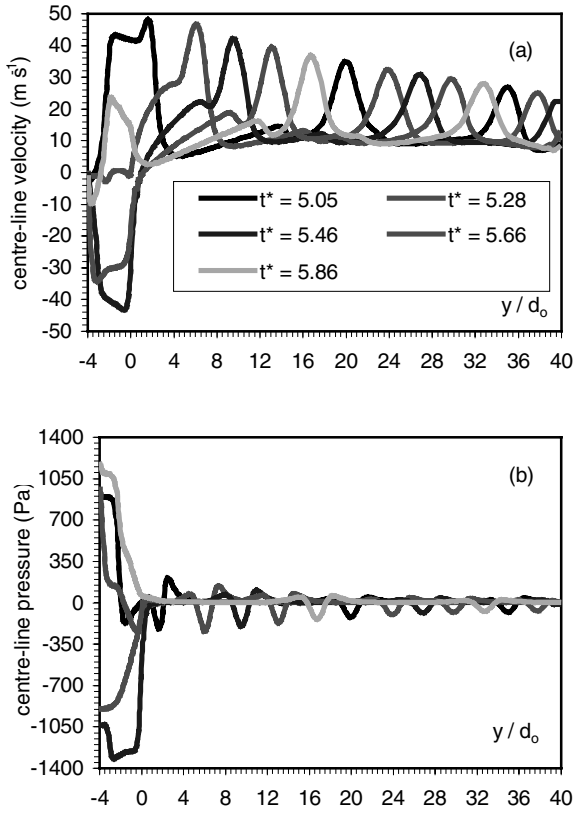

Figure 3. Instantaneous centre-line distributions. (a) stream-wise velocity; (b) pressure.

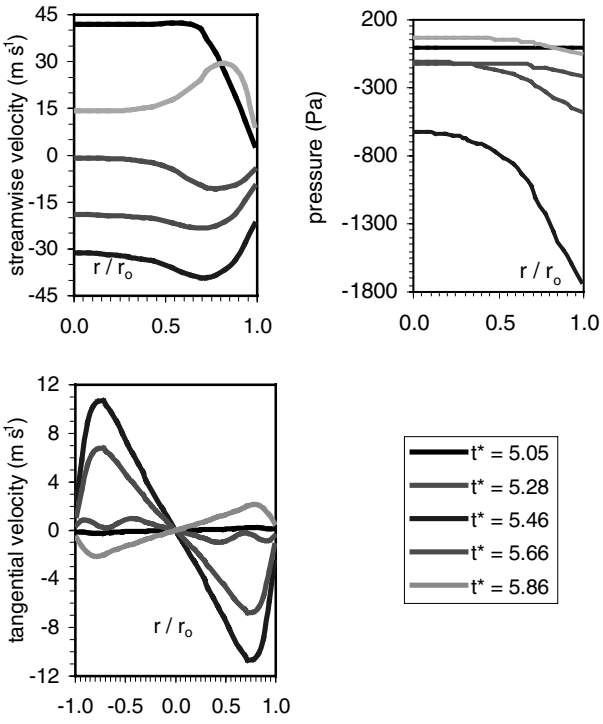

Figure 4. Instantaneous distributions across the orifice exit plane, y / d_o = 0. (a) stream-wise velocity; (b) pressure; (c) tangential velocity. NB: (a) and (b) are symmetric about r = 0.

series of peaks and troughs due to the cyclic passage of vortices. It can be seen that the disturbances due to the main and satellite vortex rings dissipate as they proceed downstream.

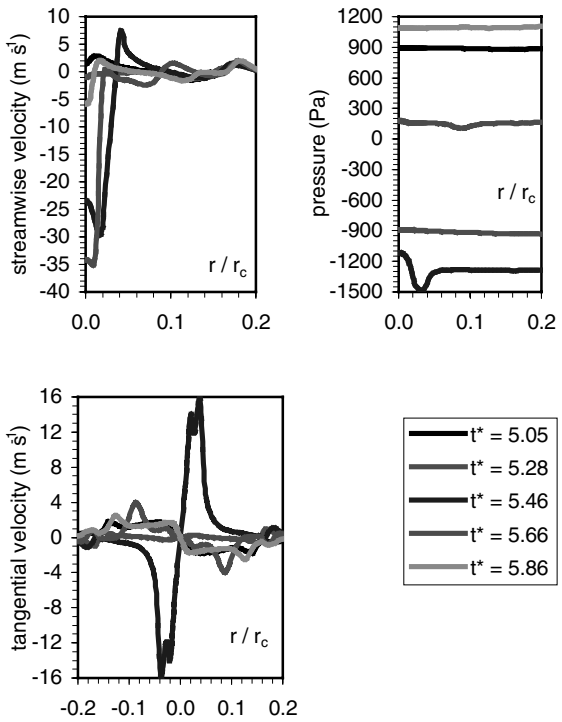

Figure 5. Instantaneous distributions across cavity mid-plane, y / d_o = -3.1.

Turbulent simulations that ignore the cavity [9] and experiments with high Reynolds number turbulent synthetic jets [14] have observed reversed flow on the centre-line to be restricted to a small region near the orifice. Here, the velocity distributions show that flow reversal only occurs for y / d_o < 1. The peak velocity in the external flow is about 5% less than is predicted by the Bernoulli equation for the maximum pressure difference between the cavity and external regions, which is approximately 1300 Pa. This difference is of the same order as friction losses across the orifice [4].

Profile distributions of stream-wise velocity, pressure and tangential velocity are shown for the orifice exit plane, y / d_o = 0, the cavity mid-plane, y / d_o = -3.1, and in the external flow at y / d_o = 5, which is just upstream of the vortex detachment location, in Figs. 4-6, respectively. For the orifice exit plane, the stream-wise velocity exhibits strong peaks and troughs towards the edge of the orifice, whilst the tangential velocity can approach fifty percent of the corresponding stream-wise value. These profiles are dramatically different to the top-hat profile assumed in earlier simulations [7,9]. The pressure profile at this location shows that a strong pressure gradient causes suction to occur along the edge of the orifice. Inside the cavity, most of the velocity variation occurs in the central twenty percent. The pressure is, however, nearly constant across the diameter, except near the mid-point of the cycle, for which there is a central peak with troughs in the wings. This is caused by the passage of the ingested vortex. At y / d_o = 5, the stream-wise profiles vary rapidly with time and are, on average, similar to those for a steady laminar jet. The pressure and tangential velocity only show significant variance during the passage of the main vortex.

The stream-wise velocity at the centre of the orifice exit is compared in Fig. 7 for cases 1-6. The maximum velocity, U_{max}, increases with increasing frequency and membrane deflection. It is also interesting to note that at the higher frequency, the temporal profile appears to steepen. All of the configurations have an offset velocity - the average of the absolute values of

maximum and minimum velocity - that is greater than zero. This indicates that on the centre-line, the actuator spends most of the cycle ejecting rather than ingesting. This concurs with the flow-field images, which suggest that most of the suction occurs near the edge of the orifice.

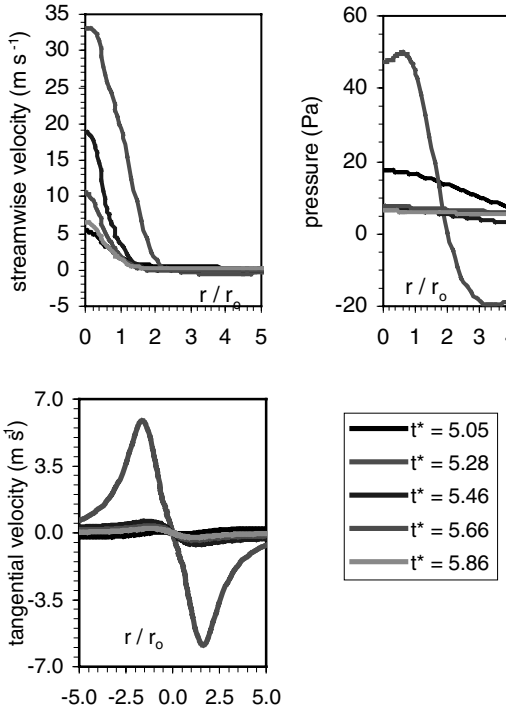

Figure 6. Instantaneous distributions at $y / d_o = 5$. (a) stream-wise velocity; (b) pressure; (c) tangential velocity.

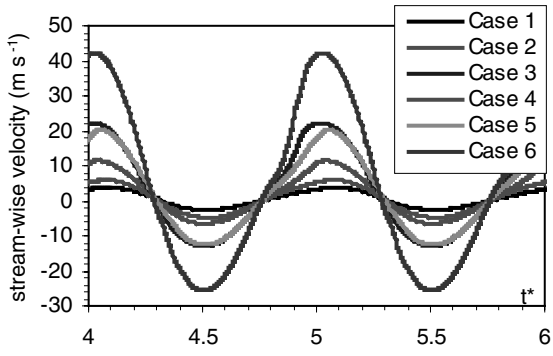

Figure 7. Temporal variation of velocity at centre of orifice exit for cases 1-6.

In terms of a control system, we need to be able to synthesize the results into readily computable forms. Figure 8 presents the variation of the output (U_{max}) with the input ($f\,\Delta_{max}$) for this actuator. This shows that the relationship between these parameters is very close to linear. This is consistent with other proposed scalings [13,14], but here the output is purely a function of the input parameters.

Conclusions

A series of numerical simulations of synthetic jet actuator flow have been performed which include realistic orifice and cavity dimensions and membrane forcing parameters. There is a strong coupling between the cavity and external flows. The external shed vortex moves away from the orifice and a satellite vortex breaks away in the later stages of the cycle. Fluid is ingested mainly along the edge of the orifice, and the fluid motion is concentrated near the centre-line of the cavity. The pressure in the cavity is, however, nearly constant span-wise at each instant in the cycle. In reality, there are likely to be strong three-dimensional effects, as even steady jets can develop asymmetric instabilities [3]. The maximum centre-line velocity varies linearly with membrane forcing frequency and maximum deflection. In future studies, we plan to see whether similar relationships hold when orifice and cavity dimensions are varied, and to extend our computations to three-dimensions.

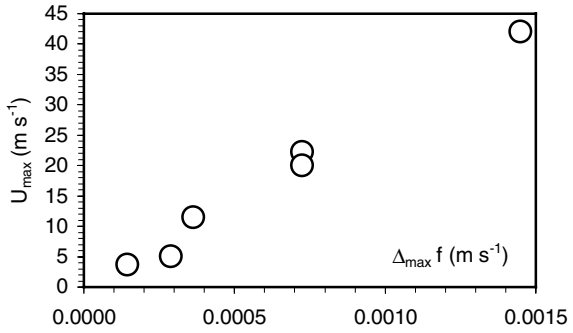

Figure 8. Variation of maximum velocity at the centre of the orifice exit plane with product of membrane deflection and frequency.

References

[1] Blevins, R.D., *Formulas for Natural Frequency and Mode Shape*, Kreiger Publishing, 1984.

[2] Cater, J. and Soria, J., Comparison between Axi-Symmetric Zero-Net-Mass Flux Jets and Continuous Jets. *Proc. 7th Australasian Heat and Mass Transf. Conf.*, QLD, 2000.

[3] Danaila, I. and Boersma, B.J., Mode Interaction in a Forced Homogeneous Jet at Low Reynolds Numbers, *Proc. Summer Prog. 1998*, *CTR-Stanford*, 1998, 141-158

[4]Gravesen, P., Branebjerg, J. and Jensen, O. S., Microfluidics – a Review, *J. Micromech. And Microeng.*, **3**, 1993, 168-182.

[5] Guo, D.G. and Kral, L.D., Numerical Simulation of the Interaction of Adjacent Synthetic Jet Actuators, *AIAA paper* 2000-2565, 2000.

[6] Horrocks, G.D., Reizes, J.A. and Hong, G., Tumble Vortex Breakdown During the Compression Stroke of a Model Internal Combustion Engine, *ASME I.C.E Div. Paper* 2000-ICE-303, 2000.

[7] Kral, L.D., Donovan, J.F., Cain, A.B. and Cary, A.W., Numerical Simulations of Synthetic Jet Actuators, *AIAA paper* 97-1824, 1997.

[8] Lee, C.Y. and Goldstein, D.B., Two-Dimensional Synthetic Jet Simulation, *AIAA paper* 2000-0406, 2000.

[9] Mallinson, S.G., Reizes, J.A. and Hong, G., An Experimental and Numerical Study of Synthetic Jet Flow, *Aeronautical J.*, **105**, 2001, 41-49.

[10]Mallinson, S.G., Reizes, J.A., Hong, G. and Westbury, P.S., Analysis of Hot-Wire Anemometry Data Obtained in a Synthetic Jet Flow. Submitted to *Exp. Thermal and Fluid Sci.*, 2001.

[11] Mittal, R., Rampunggoon, P., Udaykumar, H.S., Interaction of a Synthetic Jet with a Flat Plate Boundary Layer, *AIAA paper* 2001-2773, 2001.

[12] Rizzetta, D.P., Visbal, M.R., and Stanek, M.J., Numerical Investigation of Synthetic Jet Flowfields, *AIAA paper* 98-2910, 1998.

[13] Smith, B.L. and Glezer, A., The Formation and Evolution of Synthetic Jets, *Phys. Fluids*, **10**, 1998, 2281-2297.

[14] Smith, B.L. and Swift, G.W., Synthetic Jets at Large Reynolds Number and Comparison to Steady Jets, *AIAA paper* 2001-3030, 2001.